

A Flow Structure Interaction Method for Towed Cable System

Wang Zhi-bo^{1,*}, Huang Shuai-yu¹ and Gu Jin-Jing¹

¹School of ocean engineering, Jiangsu Ocean University, Lianyungang, Jiangsu, 222005, China

Abstract: The ocean towed cable system is a classic example of fluid-structure interaction (FSI). This interaction can exhibit stability or oscillation between a highly deformable moving cable and the surrounding turbulent flow. However, in dynamic simulations of towed cable systems, a constant drag coefficient for an infinite circular cylinder is often used based on experimental data. An innovative fluid-structure interaction method is introduced to obtain accurate drag distribution along cable to couple with towed system dynamics. A modified nodal position finite element method (NPFEM) coupled with Reynolds-averaged Navier-Stokes (RANS) approach has been utilized to predict hydrodynamic forces along the cable. A data exchange algorithm has been developed specifically for fluid-structure interaction within the towed cable system where the cable profile is transferred to construct the flow domain while hydrodynamics is interpolated for NPFEM analysis. A topology partition around cable is applied. A multiblock grid is generated around cable. The simulation results of the fluid-structure interaction of the towing system are verified. This FSI scheme reveals how strongly hydrodynamics determine cable dynamics and induce vortex structure vibrations around a towed cable system. Parametrically controlled structured grid generation and their applicability for complex flow fields have also been discussed. Detailed descriptions of boundary layer separation evolution around spatially distributed cable are provided. This FSI scheme reveals a real strongly hydrodynamic determined cable dynamics and vortex structure induced vibrations around a towed cable system. The proposed method enhances predictive accuracy of the towed system dynamics response.

Keywords: Towed Cable System, Nodal Position Finite Element Method, Reynolds Averaged Navier Stokes Equations, Boundary Layer Separation, Flow Structure Interaction.

INTRODUCTION

A towed cable system has a large flow field around cable. The deformable cable shape is totally determined by hydrodynamic load at given towing speed and length of cable and many other towed body parameters according to Kundu [1]. The Reynolds number $Re = U_{ref} D/v$ is defined in terms of the cable diameter D and the free-stream velocity U_{ref} . However, ocean towed cable often has a Reynolds number between 10^4 and 10^5 . The structure of wake behind a circular cylinder is a well investigated fluid dynamics problem, with vast data for validation. Cable wake characteristics is between flow states and patterns around ellipse and cylinder. This wake is also dominated in terms of the vortex formation and shedding, wake structure and evolution, boundary layer separation and shear layer.

Kundu [1] also pointed out there is no significant regular wake structure in wake of cylinder or ellipse within Re , but there is a relatively stable boundary layer separation locations at the leading edge of cylinder. Some efforts have been made to build the connection between flow field and cable dynamics including multiphase interpolation and transformation. Du [2] obtained drag force on lumped towed sonar cable array by calculating the drag force in the flow field of the underwater vehicle and its propeller, which is computed

by CFD methods. Yang [3] considered that hydrodynamics on towed cable was determined by the real-time velocities of the flow field at the nodes connecting the cable segments.

Also, numerical refinement such as adaptive distribution of cable elements, algorithm corrections, cut-and-try hydrodynamics prediction for a towing tank validation case or sea trial data can be found in Zhao [4], Guan [5], and Wu [6]. Many other researchers adopt various drag coefficients along towed cable as shown in Table 1. Distribution of statistical values of Table 1 indicates a totally different cable profile of the same towing parameters. Nevertheless, A selection of drag coefficients decides towing performance because of one-way load transfer to cable. It is necessary to obtain varying boundary separation, shear layer and vortex shedding in wake behind curved cable. However, Grosenbaugh [7], Wang [8], Kishore [9], and Gao [10] calculated the hydrodynamic loads of towed cable with constant drag coefficient in turning maneuver. A direct fluid and structure scheme is developed for substantial hydrodynamic distribution along towed cable in this paper. This scheme includes highly efficient flow field simulation and open frame of towed cable dynamic model.

This one-way FSI scheme is built by using open frame finite element method NPFEM given by Sun [11] and Zhu [12] to simulate cable dynamics and a modified RANS code based on SU2. A design of data transfer includes cable profiles and hydrodynamic interpolation at each time step.

*Address correspondence to this article at the School of ocean engineering, Jiangsu Ocean University, Lianyungang, Jiangsu, 222005, China; E-mail: wwzb3@163.com

Table 1: Statistical Hydrodynamic Coefficient

NO.	Reference	C_t	C_n	C_n/C_t
1	Zhu [12]	0.01	1.2	120
2	Guan [5]	0.01~0.031	1.2~2.0	200
3	Gao [10]	0.01	1.2	120
4	Wu [20]	0.02	2.0	100
5	Park [19]	0.01	0.93~0.95	95
6	Du [2]	0.03	1.2	40
7	Huang [16]	0.01	1.2	120
8	Yang [3]	0.0035	0.2297	65.6
9	Grosenbaugh [7]	0.02	2.0	100
10	Srivastava [18]	0.015,0.0089,0.0216	1.8,2.0	133.3
11	Zhao [4]	0.1	1.7	17
12	Luis [21]	0.01	1.2	120
13	Wang [17]	0.018,0.023	1.29,1.57	87.2

1. FLOW STRUCTURE COUPLING METHOD

1.1. Cable Dynamics System

Similar to cable dynamic framework built by Sun [11] and Zhu [12], we use virtual work principle to rederive the NPFEM, and establish a global coordinate system with the surface end of towed cable as coordinate origin, the water depth direction as the -Z direction, the mothership tow maneuver located in the XOY plane, and towing direction is along +X axis. The element position is described by nodal coordinates (X_i, Y_i, Z_i) ($i = 1, 2$) in the global coordinate system as shown in Figure 1. Local coordinates x, y and z are defined within x -axis along cable axis, y and z perpendicular to the x -axis, respectively. It is also assumed that node position \mathbf{R} , node velocity \mathbf{V} and the acceleration \mathbf{a} are expressed in terms of shape functions and nodal coordinates in equation (1).

$$\mathbf{R} = N\mathbf{X}_e$$

$$\mathbf{v} = \dot{\mathbf{R}} = N\dot{\mathbf{X}}_e$$

$$\mathbf{a} = \ddot{\mathbf{R}} = N\ddot{\mathbf{X}}_e \quad (1)$$

where

$$N = \begin{bmatrix} 1-\zeta & 0 & 0 & \zeta & 0 & 0 \\ 0 & 1-\zeta & 0 & 0 & \zeta & 0 \\ 0 & 0 & 1-\zeta & 0 & 0 & \zeta \end{bmatrix}$$

$$\zeta = \frac{((X - X_1)^2 + (Y - Y_1)^2 + (Z - Z_1)^2)^{1/2}}{((X_2 - X_1)^2 + (Y_2 - Y_1)^2 + (Z_2 - Z_1)^2)^{1/2}}$$

$\mathbf{R}=\{X, Y, Z\}^T$, $\mathbf{v}=\{v_x, v_y, v_z\}^T$, $\mathbf{a}=\{a_x, a_y, a_z\}^T$, are the global position, global velocity and acceleration vectors of arbitrary point along the element, respectively.

$$\mathbf{X}_e = [X_1 \ Y_1 \ Z_1 \ X_2 \ Y_2 \ Z_2]^T$$

\mathbf{X}_e is the global coordinate vector of nodes, $\dot{\mathbf{X}}_e$ and $\ddot{\mathbf{X}}_e$ indicate the first and second order derivatives to time, and N is the element shape function.

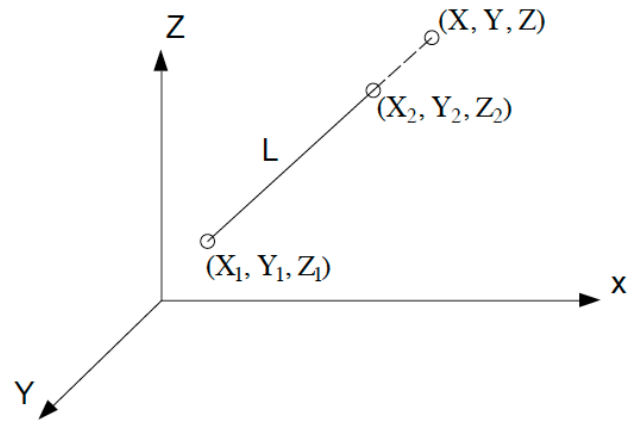


Figure 1: Nodal coordinates of a cable element.

Let L and L_0 are the length of the deformed and undeformed element. The elastic strain is calculated by deformation in direction of element axis with stretched length to calculate the relative elongation as equations (2) and (3).

$$\varepsilon = \frac{L}{L_0} - 1 = \frac{L^2}{L_0 L} - 1 \quad (2)$$

$$\varepsilon = \frac{X_2 - X_1}{L_0} \cos\theta_X + \frac{Y_2 - Y_1}{L_0} \cos\theta_Y + \frac{Z_2 - Z_1}{L_0} \cos\theta_Z - 1 = B_0 Q X_e - 1 \quad (3)$$

where $\varepsilon = \frac{T}{EA}$ is regarded as axial strain, where

$$\cos\theta_X = \frac{X_2 - X_1}{L} \quad \cos\theta_Y = \frac{Y_2 - Y_1}{L} \quad \cos\theta_Z = \frac{Z_2 - Z_1}{L}$$

θ_X θ_Y θ_Z indicate spatial azimuths of a cable element in a global coordinate.

$$B_0 = [-1/L \quad 0 \quad 0 \quad 1/L \quad 0 \quad 0]$$

Q is the coordinate transformation matrix from local to global coordinate system, Q is 6×6 matrix, where nonzero elements are $Q_{1,1} = Q_{4,4} = \cos\theta_X$ $Q_{1,2} = Q_{4,5} = \cos\theta_Y$, $Q_{1,3} = Q_{4,6} = \cos\theta_Z$.

where length of element after deformation is the distance between two nodes:

$$L = ((X_2 - X_1)^2 + (Y_2 - Y_1)^2 + (Z_2 - Z_1)^2)^{1/2}$$

The expression for the strain energy of the element can be discreted as

$$U = \frac{1}{2} \int_0^L EA \varepsilon^2 ds = \frac{1}{2} X_e^T K X_e - X_e^T F_K + \frac{1}{2} EAL \quad (4)$$

where E is Young's modulus of the cable element, A is cross section area of the cable element, F_K is the generalized nodal force vector resulting from the elasticity of the cable element, and K is stiffness matrix which conversion from local to global coordinate system.

$$K = EAL(B_0 Q)^T B_0 Q = Q^T K_0 Q$$

The stiffness matrix in local coordinate system is written as

$$K_0 = K_{01} L / L_0$$

$$K_{01} = \begin{bmatrix} 1 & 0 & 0 & -1 & 0 & 0 \\ 0 & 0 & 0 & 0 & 0 & 0 \\ -1 & 0 & 0 & 1 & 0 & 0 \\ O_{3 \times 3} & & & O_{3 \times 3} & & \end{bmatrix}$$

$$F_K = EAL Q^T B_0^T$$

It is worth noted that stiffness matrix K_{01} is a two-node stiffness matrix, and K_0 is considered with scaling factor L/L_0 , for small strain deformations has $L/L_0 = 1 + \varepsilon$.

The kinetic energy of the element can be written as

$$T = \frac{1}{2} \int_0^L \rho \dot{R}^T \dot{R} dx = \frac{1}{2} \dot{X}_e^T M \dot{X}_e \quad (5)$$

$$\text{where } M = \frac{\rho AL}{6} \begin{bmatrix} 2I_{3 \times 3} & I_{3 \times 3} \\ I_{3 \times 3} & 2I_{3 \times 3} \end{bmatrix}$$

where M is the mass matrix of cable element in global coordinate and ρ is the material density. It should be noted that the element mass matrix is the constant in the global coordinate system and is the same as the consistent mass matrix of the cable element in the existing finite element method.

The virtual work done by the inertial force of the added mass effect is given by

$$\delta W_a = - \int_0^L f_a^T \cdot \delta R dx = \delta X_e^T \cdot M_a \cdot \ddot{X}_e - \delta X_e^T \cdot F_a \quad (6)$$

$$M_a = \frac{1}{6} C_m \rho_0 AL (M_{a0} - M_{a1})$$

$$F_a = M_a \dot{V}_c^e \quad M_{a0} = 2I_{6 \times 6} \quad M_{a1} = \begin{bmatrix} 2m_0 & m_0 \\ m_0 & 2m_0 \end{bmatrix}$$

$$m_0 = \begin{bmatrix} \cos^2 \theta_X & \cos \theta_X \cos \theta_Y & \cos \theta_X \cos \theta_Z \\ \cos \theta_X \cos \theta_Y & \cos^2 \theta_Y & \cos \theta_Y \cos \theta_Z \\ \cos \theta_X \cos \theta_Z & \cos \theta_Y \cos \theta_Z & \cos^2 \theta_Z \end{bmatrix}$$

where M_a is the added mass matrix resulting from the fluid surrounding the element, F_a is inertial force vector due to the added mass of the fluid surrounding the element, $I_{6 \times 6}$ is unity matrix.

$$\dot{V}_c^e = [\dot{V}_{cx1}^e \quad \dot{V}_{cy1}^e \quad \dot{V}_{cz1}^e \quad \dot{V}_{cx2}^e \quad \dot{V}_{cy2}^e \quad \dot{V}_{cz2}^e]^T$$

\dot{V}_c^e is the fluid acceleration vector at the element nodes.

Added mass matrix and the inertial force vector are considered as highly nonlinear and time-dependent, because node position of element is time-varying. All these virtual works mentioned above are defined in global coordinate system.

Therefore, the virtual work done by the drag forces is given by

$$\delta W_d = - \int_0^L f_d^T \cdot \delta r dx = - \delta x_e^T \cdot f_d^e \quad (7)$$

where f_d^e is the equivalent nodal drag forces in the local coordinates.

Drag force vector f_d^e needs to be transformed to global coordinate system.

$$\delta W_d = - \delta x_e^T \cdot f_d^e = - \delta X_e^T \cdot F_d \quad (8)$$

where $F_d = T^T f_d^e$

T^T is coordinate transformation matrix between local and global coordinate system. Last, virtual work done by buoyant and gravity is also defined in global coordinate system, assuming that gravity force is -z vertically downward and the virtual work done by the force is

$$\delta W_{bg} = \int_0^L Ag[0 \quad 0 \quad \rho - \rho_0] \cdot \delta R dx = -\delta X_e^T \cdot F_{bg} \quad (9)$$

where g is acceleration due to gravity and F_{bg} is the equivalent nodal buoyant and gravity force vector, as follows:

$$F_{bg} = \frac{1}{2} LA(\rho - \rho_0)g[0 \quad 0 \quad 1 \quad 0 \quad 0 \quad 1]^T$$

Now, we can derive the equation of motion of the element using the principle of virtual work, such that

$$\delta(U - T) + \delta W_a + \delta W_d + \delta W_{bg} = 0 \quad (10)$$

Substituting Equations (4), (5), (6), (8), and (9) into Equation (10) leads to the equation of motion as:

$$\delta X_e^T \cdot ([M + M_a]\ddot{X}_e + KX_e - F_K - F_a - F_d - F_{bg}) = 0$$

Since there is damping in any structural system, we introduce a damping matrix into the equation of motion.

$$[M + M_a]\ddot{X}_e + C\dot{X}_e + KX_e = F_K + F_a + F_d + F_{bg}$$

The damping matrix C is calculated using Rayleigh damping model, such that

$$C = \beta[M + M_a] + \gamma K \quad (11)$$

Let $F = F_k + F_a + F_d + F_{bg}$, the equation of motion in Equation (12) is highly nonlinear because the matrices of added mass, damping, and stiffness on the left-hand side and the force vectors on the right-hand side are the functions of the current position X_e and velocity \dot{X}_e , respectively.

$$[M + M_a]\ddot{X}_e + C\dot{X}_e + KX_e = F \quad (12)$$

In this study, the towed body is simplified to a mass point model, without considering the rotation of the towed body, the towed body is subject to gravity, buoyancy, drag force and additional mass force, as well as the draft tension. The motion of the towed cable satisfies:

$$[M_d + M_{da}]\ddot{X}_d + C_d\dot{X}_d + K_dX_d = F_T + F_{dg} + F_D \quad (13)$$

Combination of (12) and (13) above can be assembled to obtain the overall stiffness matrix, damp matrix and mass matrix, as well as the source term vector.

$$[M_t + M_{ta}]\ddot{X}_t + C\dot{X}_t + KX_t = F_t \quad (14)$$

These systems can be discrete into a set of quadratic equations such as equation (15), we use a numerical package IMSL [13] which is integrated with Newmark time scheme.

$$\begin{aligned} K_{t+\Delta t}X_{e_{t+\Delta t}} &= \left(\frac{M}{\alpha\Delta t^2} + \beta\frac{C}{\alpha\Delta t} + K\right)u_{t+\Delta t} \\ &= M\left[\frac{1}{\alpha\Delta t^2}X_{e_t} + \frac{1}{\alpha\Delta t}\dot{X}_{e_t} + \left(\frac{1}{2\alpha} - 1\right)\ddot{X}_{e_t}\right] + \\ &C\left[\frac{\beta}{\alpha\Delta t}X_{e_t} - \left(1 - \frac{\beta}{\alpha}\right)\dot{X}_{e_t} - \left(1 - \frac{\beta}{2\alpha}\right)\ddot{X}_{e_t}\right] + F_{t+\Delta t} \end{aligned} \quad (15)$$

1.2. Construction of Computational Fluid Dynamics Module

Flow field should be able to accurately and efficiently simulate a separated boundary flow around towed cable. A cable is considered as a smoothed surface with circular cross-section. There is a large scale of separate vortex in flow field within commonly used towing speed range. According to Wilcox [14], we use Reynolds Averaged Equations to approximate Navier-Stoke equations. The Reynolds averaged velocity field U_i can be modeled as equation (16) and (17).

$$\frac{\partial \rho}{\partial t} + \frac{\partial \rho U_j}{\partial x_j} = 0 \quad (16)$$

$$\frac{\partial \rho U_i}{\partial t} + \frac{\partial}{\partial x_j}(\rho U_i U_j) = -\frac{\partial p}{\partial x_i} + \frac{\partial}{\partial x_j}(\tau_{ij} - \rho \overline{u_i u_j}) + S_M \quad (17)$$

where τ is molecular viscosity, $\rho \overline{u_i u_j}$ is Reynolds stress, and S_M is body force, and the relationship between the Reynolds stress and Reynolds mean velocity is established using assumption vortex viscosity assumption in equation (18).

$$-\rho \overline{u_i u_j} = \mu_t \left(\frac{\partial U_i}{\partial x_j} + \frac{\partial U_j}{\partial x_i}\right) - \frac{2}{3} \delta_{ij} \left(\rho k + \mu_t \frac{\partial U_k}{\partial x_k}\right) \quad (18)$$

where μ_t is turbulent viscosity coefficient, a model suitable from low to medium Re that can accurately capture the shear layer in a separation flow is adopted. In this study, SST turbulence model combined with gravity field is assessed, and this turbulence model is based on a turbulent viscosity μ_t , turbulent kinetic energy and turbulence frequency respectively. They have a relation as equation (19).

$$\mu_t = \rho \frac{k}{\omega} \quad (19)$$

where k is turbulent kinetic energy and ω is turbulence frequency respectively, k and ω satisfies the corresponding transport equation:

$$\frac{\partial(\rho k)}{\partial t} + \frac{\partial}{\partial x_j}(\rho U_j k) = \frac{\partial}{\partial x_j} \left[\left(\mu + \frac{\mu_t}{\sigma_{k1}} \right) \frac{\partial k}{\partial x_j} \right] + P_k - \beta' \rho k \omega \quad (20)$$

$$\frac{\partial(\rho \omega)}{\partial t} + \frac{\partial}{\partial x_j}(\rho U_j \omega) = \frac{\partial}{\partial x_j} \left[\left(\mu + \frac{\mu_t}{\sigma_{\omega 1}} \right) \frac{\partial \omega}{\partial x_j} \right] + \alpha_1 \frac{\omega}{k} P_k - \beta_1 \rho \omega^2 \quad (21)$$

These RANS model is implemented into a modified SU2 [24] code. The modification includes y+ prediction and mesh refinement. Since production of turbulent

viscosity generation is mainly from separation flow near wall boundary layer, the accurate solution of turbulence kinetic energy and turbulence frequency based on viscous mesh determines the correct calculation of separation vortex and tail vortex structure caused by turbulence viscosity. In this study, Y^+ should be less than 1.0 to fully simulate a boundary flow around cable which can satisfy accurate solution to viscous sublayer, and gravity field must be considered in this flow field.

In order to decrease computational cost, a structured grid generation strategy is designed in this study. A polynomial approximation is used to fit cable spatial profile in a towed condition. The cable shape of towed cable can be fitted as a polynomial of higher than third order $N \geq 3$:

$$l(x, y, z) = C_0 + \sum_{n=1}^N a_n x^n + b_n y^n + c_n z^n \quad (22)$$

Coefficients matrix can be obtained using a fitting linear regression method to rewritten as $A = [a_1 \ a_2 \ a_3]$ $B = [b_1 \ b_2 \ b_3]$ $C = [c_1 \ c_2 \ c_3]$.

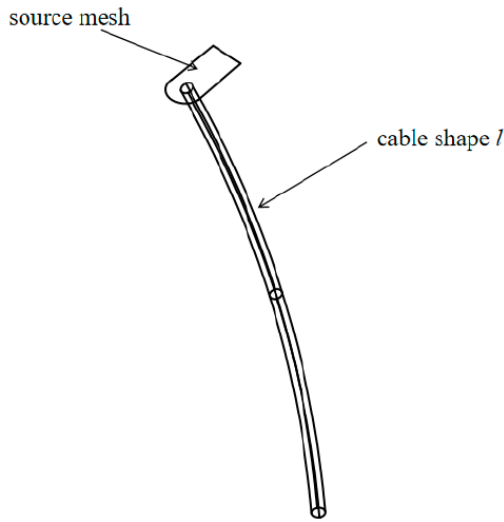


Figure 2: Mesh generation.

The diagram of interactive iterations between flow field and cable system are started as shown in Figure 3. The mesh generation method is shown in Figure 2. Based on generation of two-dimensional structured grid as source mesh. A cable shape l is considered as a guide line, initial inclination angle θ_1 of the first cable element of cable is considered as inclination angle of the plane. The cable curve is used as a guideline. Two-dimensional mesh on source plane is swept along the cable curve leads to multi block computational mesh. The flow field boundaries include velocity inlet, pressure outlet and wall boundaries as shown in Figure 4. This mesh generation process is implemented using script of Gmsh[15]. At each time step the cable curve is transferred by NPFEM, and the hydrodynamic loads acting on towed cable is simulated by CFD module.

Cable profile is updated by NPFEM with a new hydrodynamic distribution after every time step.

1.3. Quasi-Static One-Way Coupling Method

1.3.1. Quasi-Static Coupling Strategy of a Straight Tow

A steady flow field is simulated based on initial cable profile from a constant drag coefficient by NPFEM. These hydrodynamic loads F_d on cable are described as the following polynomial approximation by cable curved length $l(x, y, z)$ as in equation (23). Often the constant drag coefficient has an obvious difference with these polynomials.

$$\begin{cases} F_{dx} = f_1(l) \\ F_{dy} = f_2(l) \\ F_{dz} = f_3(l) \end{cases} \quad (23)$$

Drag coefficients such as C_b , C_x , C_y , C_z are shown in (24) on each cable segment are calculated by substituted node coordinates of cable into these polynomials in (23).

$$C_t = F_d / (\frac{1}{2} \rho V^2 L_s d)$$

$$C_x = F_{dx} / (\frac{1}{2} \rho V^2 L_s d), \quad C_y = F_{dy} / (\frac{1}{2} \rho V^2 L_s d),$$

$$C_z = F_{dz} / (\frac{1}{2} \rho V^2 L_s d) \quad (24)$$

The drag force acting on cable elements is used for NPFEM simulation, The angle of attack α and drift angle β of cable relative to sea current can also be obtained.

In these heavy tow cases, there is a high tensional load in cable and an alternating smaller lateral drag force in normal direction of plane where the towed cable is in a straight-line tow. These disturbances cannot lead a significant lateral displacement of towed cable in practice. However, it can cause consistent high frequency vibration and such vibration cannot induce relatively large amplitude vibration of towed cable. So we assume $\beta \approx 0$, and $F_{dy} = 0$. This FSI treatment in a heavy straight-line tow is called quasi-static couple.

1.3.2. One-Way Couple Method

In a straight tow, we can assume the lateral force $F_y \approx 0$. But in a turning tow, a towed cable has nearly the same drift angle as mother ship so $F_y \neq 0$. The lateral hydrodynamic loads increase significantly within a ship turn. This will cause significant torsional and twisted behavior of cable. The calculation flow chart formed by this coupling method is shown in Figure 3 in which a switch is designed to consider a straight-line tow or a turning tow.

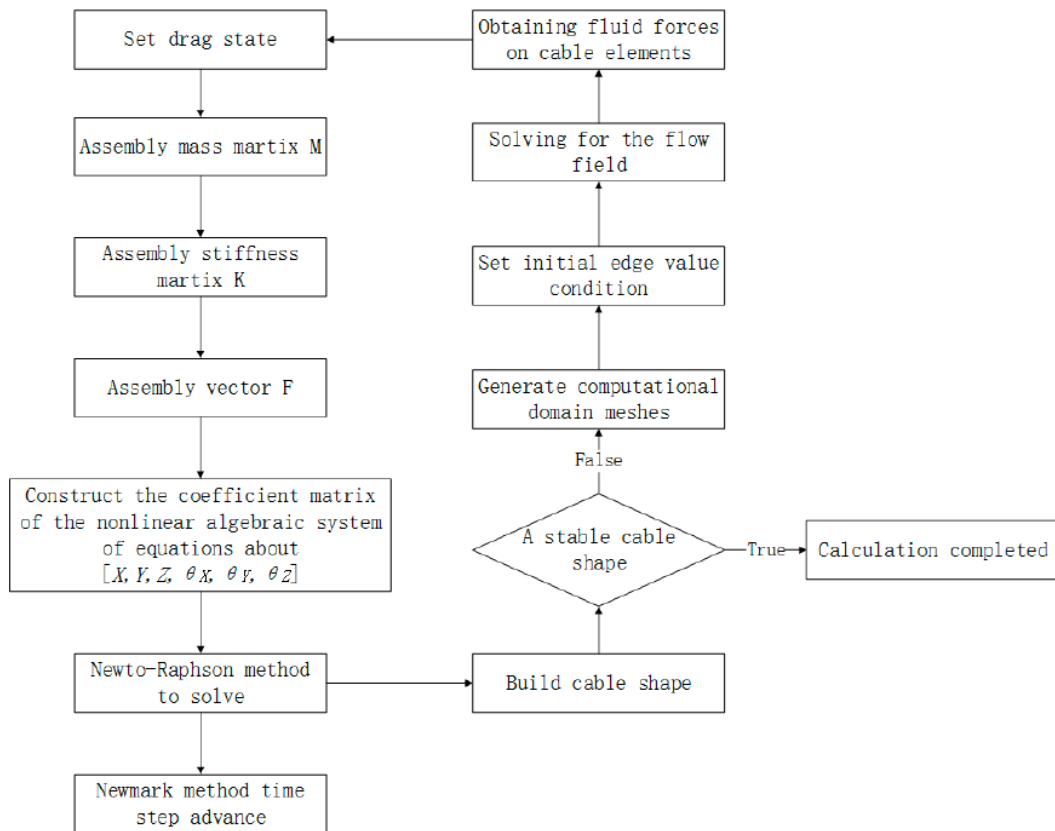


Figure 3: Diagram of FSI with NPFEM and RANS.

1.4. Mesh Generation

A structural mesh generation approach is developed for a straight tow. Figure 4 shows a flow domain design and far field boundaries around cable. Figure 5 displays a C-H shape topology surrounding cable. Area λ represents cable circular cross section, and the origin of coordinates is at point A_0 . The length of A_0B_1 , A_0C_1 , A_0C_2 , and A_0C_3 are determined by ratios to cable radius. Equations (25) and (26) can be used for the boundary layer mesh refinements. The grid point height of first layer near walls is calculated by dimensionless value of y^+ .

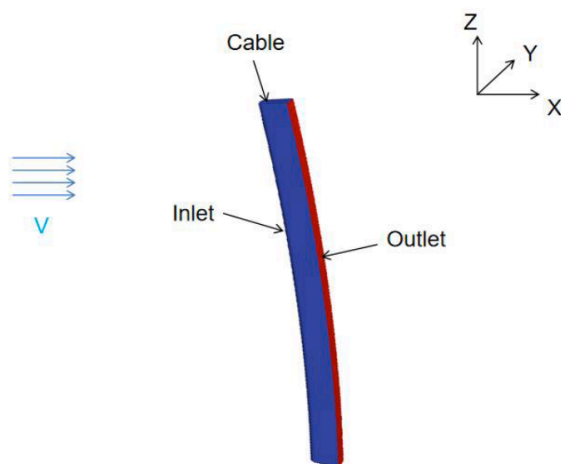


Figure 4: Domain design and boundary around cable.

$$d_s = R\sqrt{80}y^+Re^{-13/14} \tag{25}$$

$$d_{s2} = 2d_s \tag{26}$$

In Figure 4, Near wall first grid point from A_1 to B_1 is represented by d_s , and distance of the first grid point from B_1 to C_1 is represented by d_{s2} . Three-dimensional grid is generated by stretching this source topology along a cable curve. This process is implemented by using Gmsh [15] scripts.

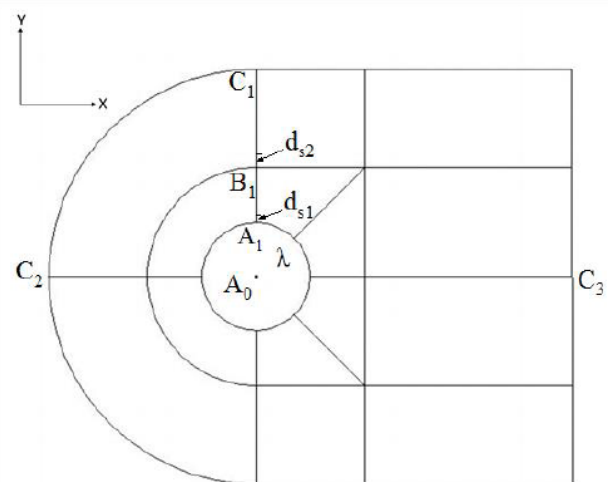


Figure 5: Design of C-H type source topology.

Table 2: Parameters of Towed System

Physical Parameters of Towed Cable		Physical Parameters of Towed Body	
Length	$L=3\text{m}$	Mass	$m=1\text{kg}$
Diameter	$D=0.01\text{m}$	Drainage volume of towed body	0.00015m^3
Density	$\rho=1050\text{kg/m}^3$	Drag coefficient	$C_{dx}=1.05, C_{dy}=0, C_{dz}=0.1$
Weight of per unit length	$\mu=0.082\text{kg/m}$	Buoyancy	1.47N
Bending stiffness	$0\text{ kN}\cdot\text{m}^2$	Towed speeds	$0.3\text{m/s}, 1.5\text{m/s}$
Poisson ratio	0.28		
Axial stiffness	110kN		
Torsional stiffness	$0\text{ kN}\cdot\text{m}^2$		
Initial C_n	1.2		
Initial C_t	0.025		

2. QUASI-STATIC SIMULATION OF A STRAIGHT TOW

2.1. Towed Cable System

A short cable system is experimentally towed in tank is carried out by Guan [5] and this towed system is used for verification of this FSI scheme. Because of a short length of towed cable, it is a small computational scale. The structure and parameters of this towed system are in Table 2.

2.2. Cable Profile and Excitation by Hydrodynamics Load

A stable towed cable shape can be obtained often after no more than two iterations as shown in Figure 6. Towed cable profile obtained in experiments by Guan [5] is basically consistent with this FSI method after two iterations. The number of iteration steps required is small. These iterative results tend to be stable. The solution error requirement is satisfied. It is a highly

efficient performance of this one-way coupling scheme. Because Guan's [5] towed cable system has a better selection of initial value approximative to the true hydrodynamic value in average. However, cable shape obtained by NPFEM with constant hydrodynamic coefficients is significantly different from the experimental results. Simulations also indicate that cable shape has flow excited oscillations due to numerical hydrodynamic loads transferred to NPFEM. A steady cable shape with a minimal oscillation interval also suggests that towed cable is susceptible controlled to the separation flow field instability.

The hydrodynamic loads have a significant influence on cable profile. Although a well guessed initial drag coefficients is implemented in this simulation, it could not adapt to increased tow speed well. Most cases show the results from FSI method agree well with experiments better in a high tow speed according to Figure 7.

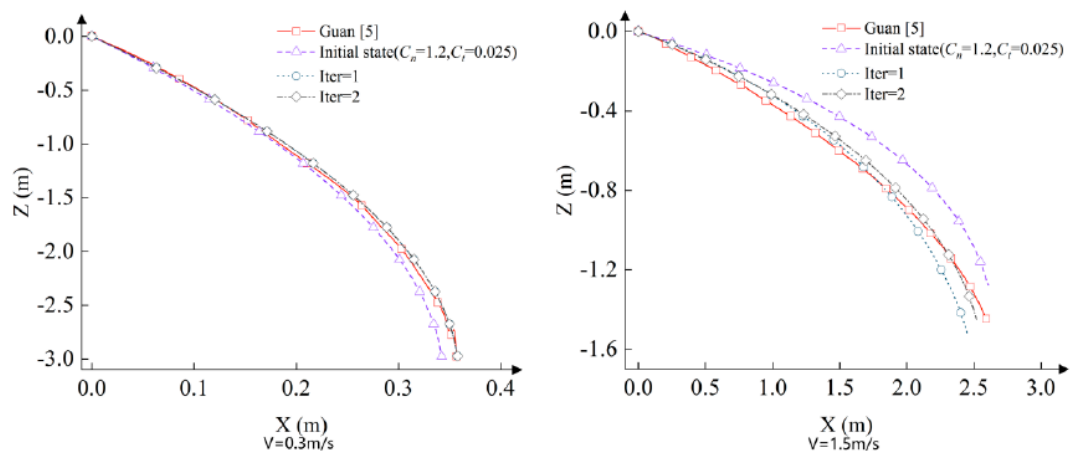


Figure 6: Convergence of iterative calculation of cable profile with two towed speed.

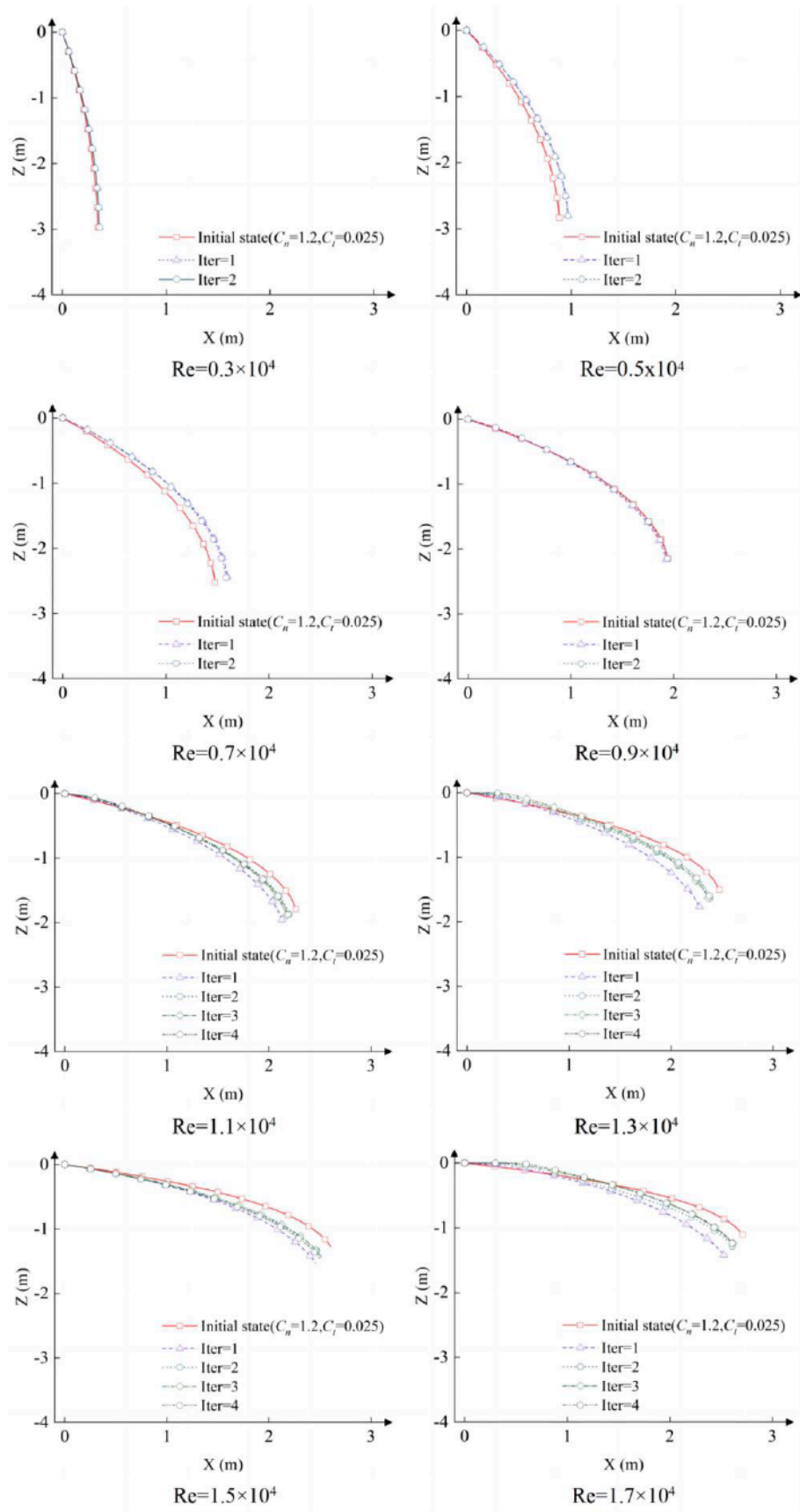


Figure 7: Convergence process of iterative calculation of cable shape with different Re.

2.3. Wake Patterns Transitions form Elliptic Flow to Cylindrical Flow

Hydrodynamics distributions of two tow velocity

along cable are shown in Figure 8 to Figure 11 in which C_dz has a significant fluctuation because elliptic cable flow wake leads a high lift effort and a cylindrical cable wake has alternately shear layer shedding, that gives

nonsignificant elevating forces but high resistances. The fluctuation in hydrodynamics along cable is more obvious in these increasing towed velocity cases.

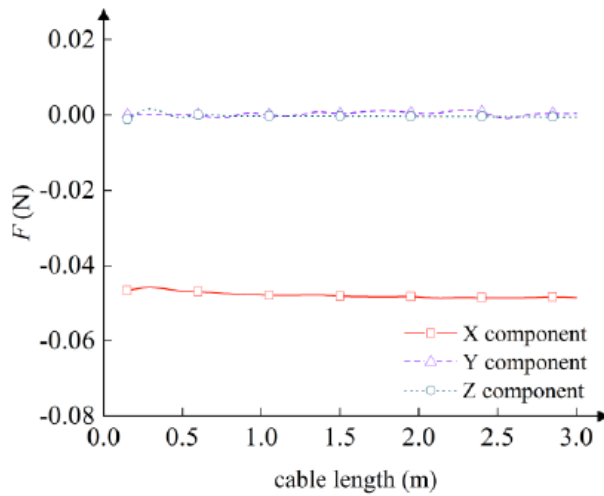


Figure 8: Distributions curve of hydrodynamic components of towed cable along cable length obtained in the last iteration ($V=0.3\text{m/s}$).

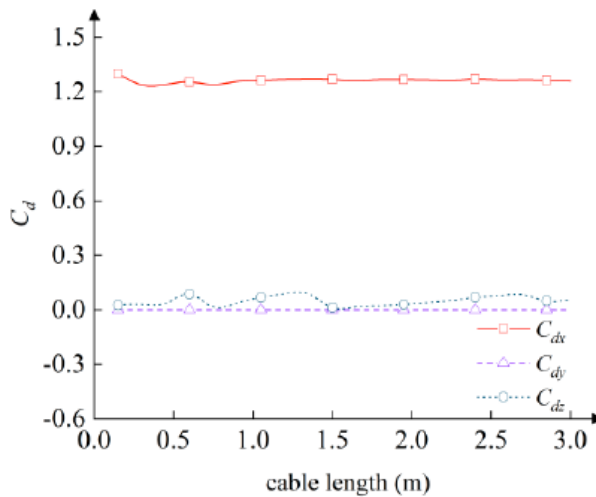


Figure 9: Distributions of drag coefficients of towed cable along cable length obtained in the last iteration ($V=0.3\text{m/s}$).

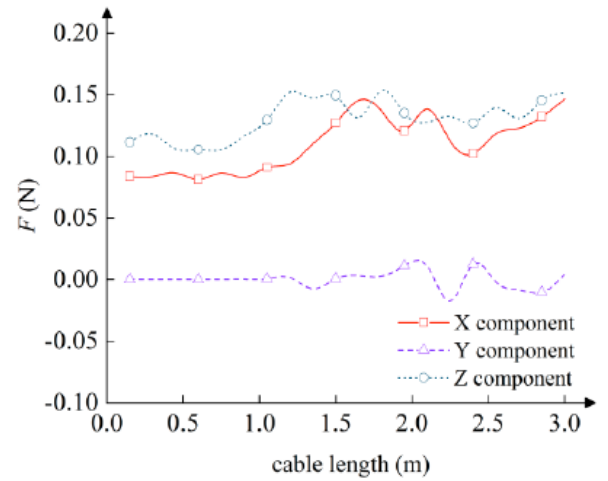


Figure 10: Distributions curve of hydrodynamic components of towed cable along cable length obtained in the last iteration ($V=1.5\text{ m/s}$).

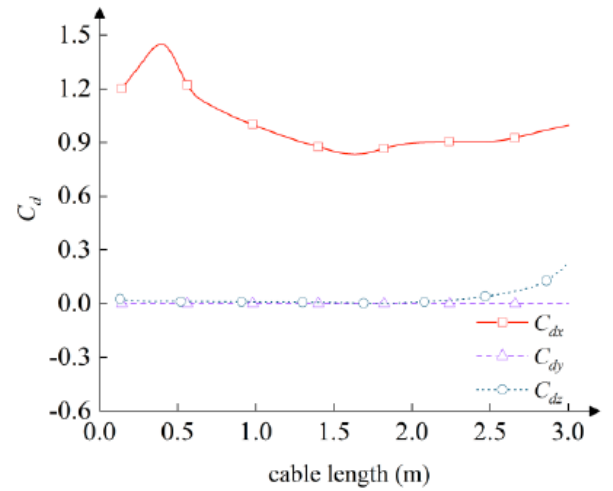


Figure 11: Distributions of drag coefficients of towed cable along cable length obtained in the last iteration ($V=1.5\text{m/s}$).

It depicts the dynamic pressure distribution of the towed cable profile in Figure 12. The z/d is used to describe the diving position of a towed cable profile. It is illustrated as an elliptic flow transition to circular cylinder along z cross section. In a low tow speed, the

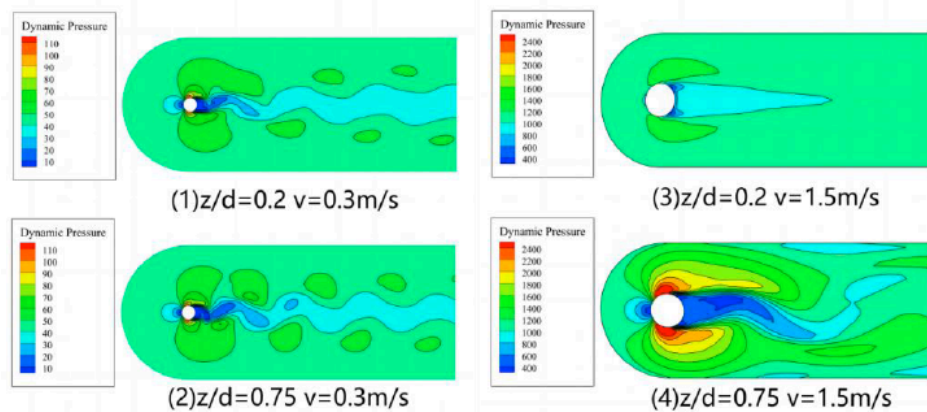


Figure 12: Towed cable wake structure at different diving depths and velocities.

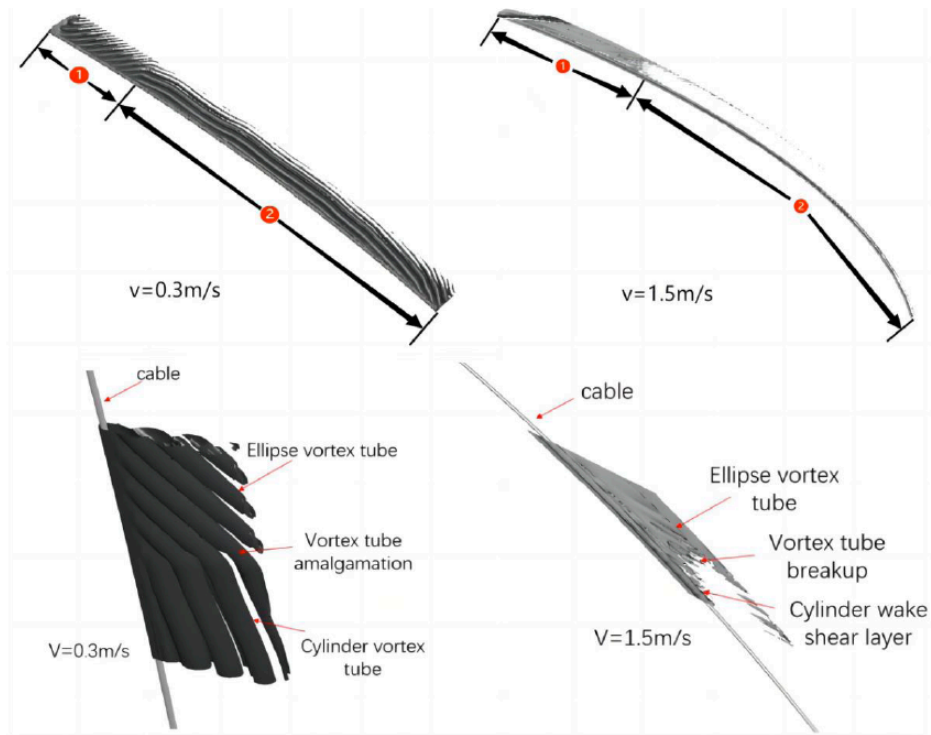


Figure 13: Contour surface of vorticity 6 s^{-1} in cable wake.

alternative vortex shedding is obviously observed in Figure 11. The cable deformation and high frequency excitation are sensitive to wake structure distribution at a high tow speed.

Figure 13 displays the contour surface of cable with vorticity of 6 s^{-1} at two towed speeds. At a towed speed of 0.3 m/s , vorticity concentration has a distribution along with incline angle of cable. Spatial frequencies of vortex shedding in wake shows an ellipse wake near surface end and a cylinder wake structure at a low speed. For a high speed of 1.5 m/s , a higher concentration of vorticity around cable can be found in Figure 13. Highly spatial vortex shedding frequencies is observed in these high speeds. However, a pair of shear layers can be found in these wake structure in Figure 12.

A large incline angle decides a ratio of major and minor axes of an ellipse. When a ratio reaches 1.0, flow around the cable has a pattern like cylinder structure. The cable wakes can be divided into two regions and their transitions. The transitional region has superimposed wake structure with vortex tube amalgamation in 0.3 m/s tow. In a high tow speed, shear layer shedding push forward and break up these column separation vortex tubes into far wakes.

2.4. Boundary Separation and Vortex Shedding Along Cable

Transient characters of flow around cable are given by spectrums of dynamic pressure. According to Figure 14 and Figure 15, dynamic pressure around cable exhibits induced vortex shedding, low frequency broadband spectrum changes no larger than 0.2 Hz .

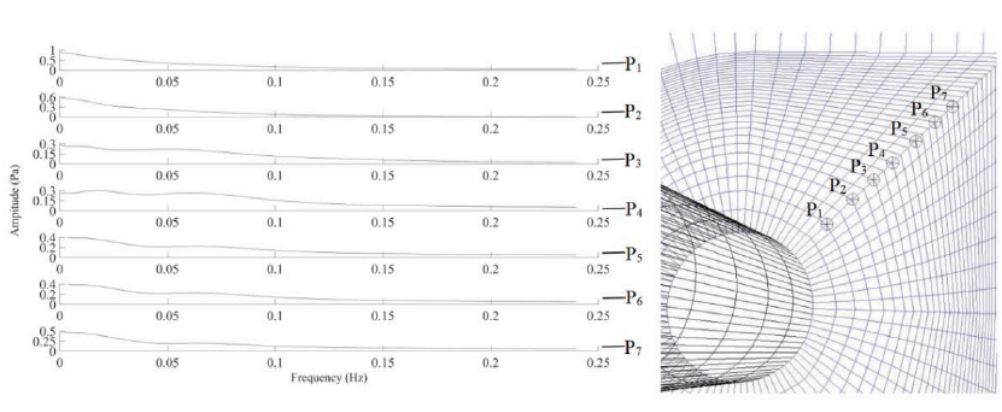


Figure 14: Spectrum of dynamic pressure converted through FFT ($V=0.3 \text{ m/s}$).

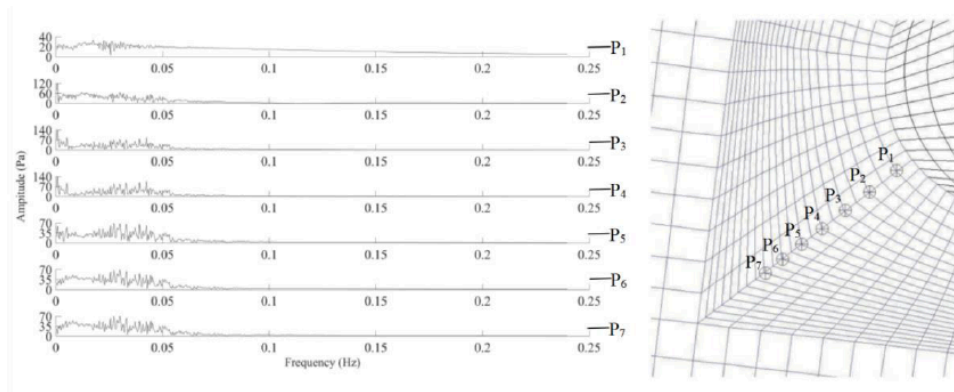


Figure 15: Spectrum of dynamic pressure converted through FFT ($V=1.5\text{m/s}$).

That means a low vortex shedding frequency range in a low tow speed. In a slow tow, high frequency vibration does not come from vortex shedding.

Figure 16 and Figure 17 display the relationship among decline angle, water depth, and separation point at different towed speeds. There are two basically symmetrical separation points around cable. According to Figure 18 to Figure 21, two symmetrical separation points around cable are more stable in elliptical flow pattern from results of FSI method.

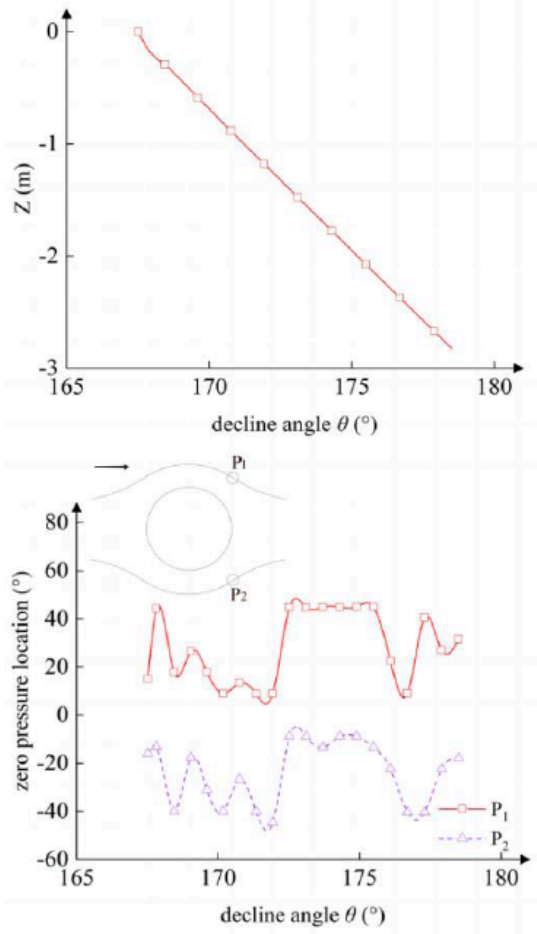


Figure 16: Separation points at $z=2.9\text{m}$ for the flow field around converged towed cable ($v=0.3\text{m/s}$).

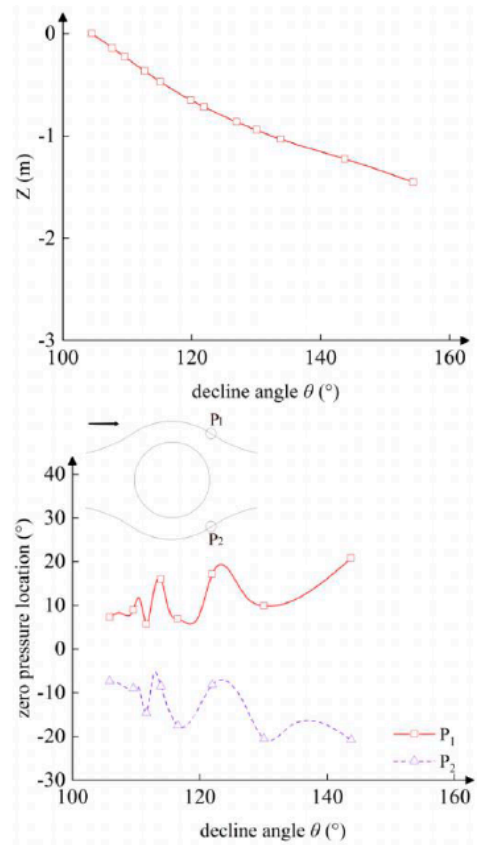


Figure 17: Separation points at $z=2.9\text{m}$ for the flow field around converged towed cable ($v=1.5\text{m/s}$).

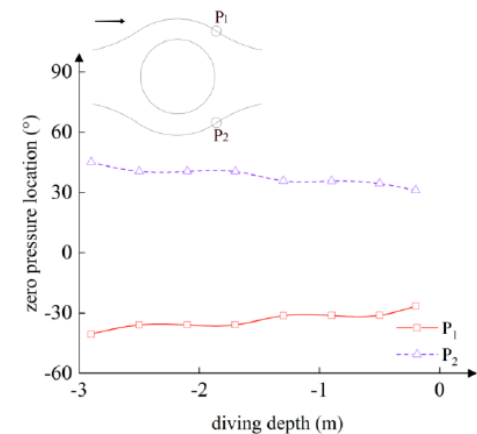


Figure 18: Polar angle of initial cable separation point along the depth ($v=0.3\text{ m/s}$).

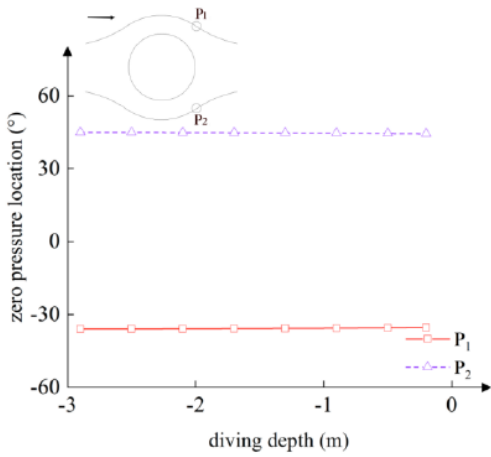


Figure 19: Pole angle of converged cable separation point along the depth ($v=0.3$ m/s).

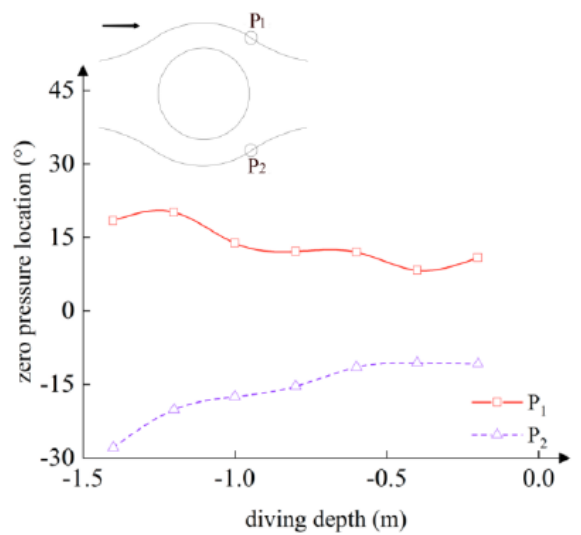


Figure 21: Pole angle of converged cable separation point along the depth ($v=1.5$ m/s).

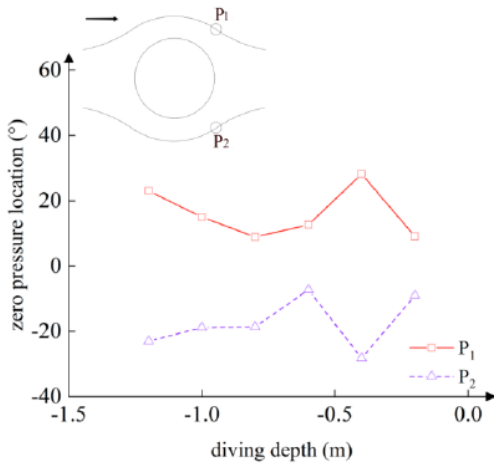


Figure 20: Polar angle of initial cable separation point along the depth ($v=1.5$ m/s).

Phase change of hydrodynamics in three directions along cable segments can be observed from Figure 22 to Figure 29. It is shown that ellipse wake has a different vortex shedding phase from a cylinder wake around cable. There is only a dominant frequency in each hydrodynamic component. And in X and Z directions a phase migration can lead a diving depth fluctuation of a towed cable. The lateral Y direction force is too small to induce a distinct lateral motion under a high tensional tow condition. Also, in the X and Z direction the drag components have the same

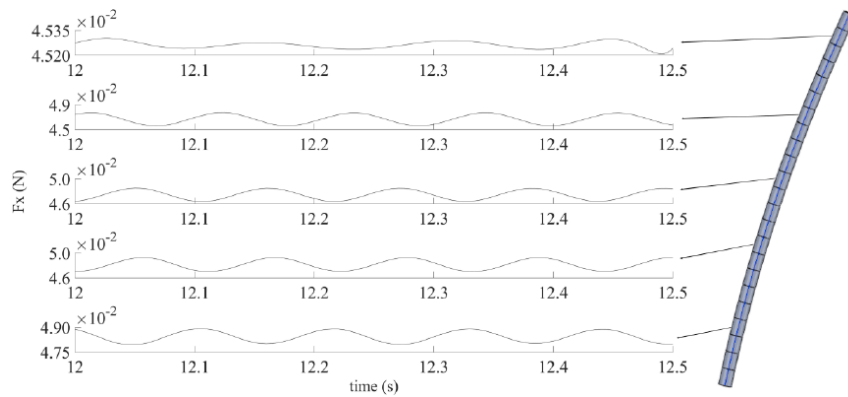


Figure 22: X-direction drag force on different wall surfaces with times ($v=0.3$ m/s).

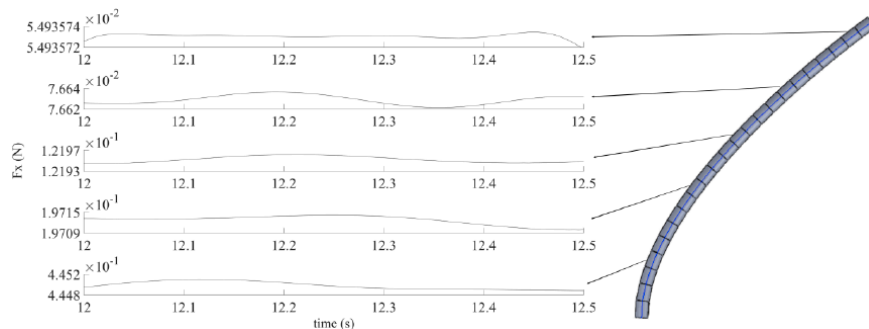


Figure 23: X-direction drag force on different wall surfaces with times ($v=1.5$ m/s).

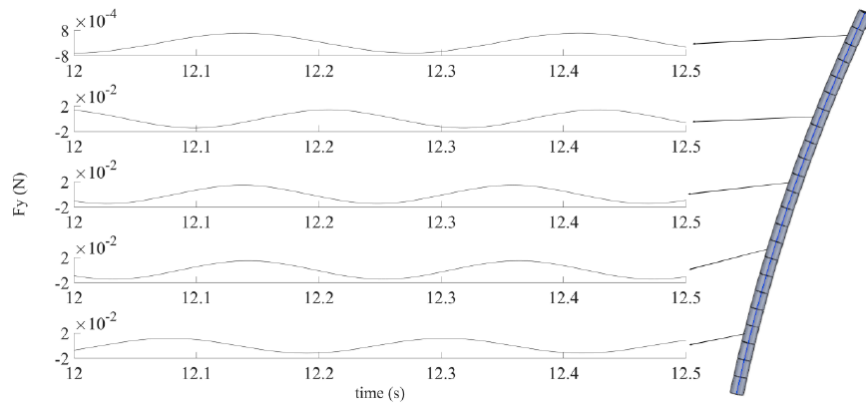


Figure 24: Y-direction lift force on different wall surfaces with times ($v=0.3\text{m/s}$).

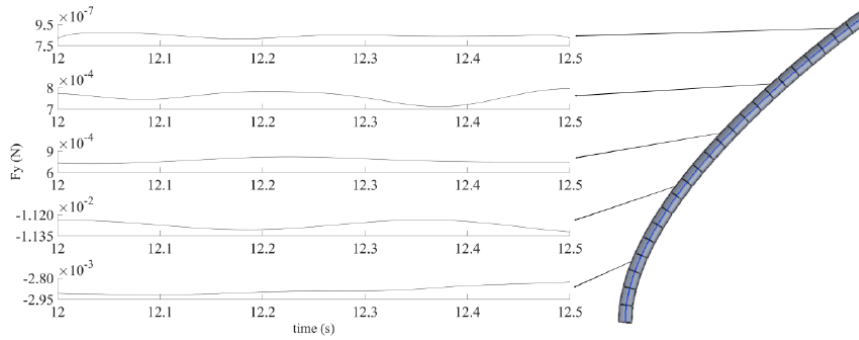


Figure 25: Y-direction lift force on different wall surfaces with times ($v=1.5\text{m/s}$).

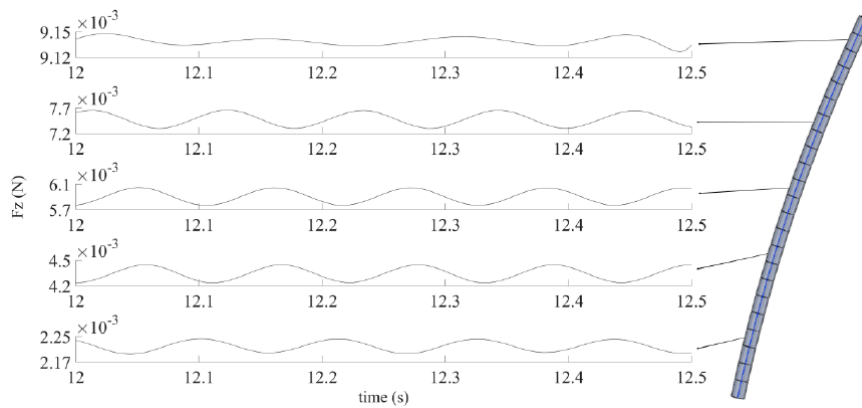


Figure 26: Z-direction drag force on different wall surfaces with times ($v=0.3\text{m/s}$).

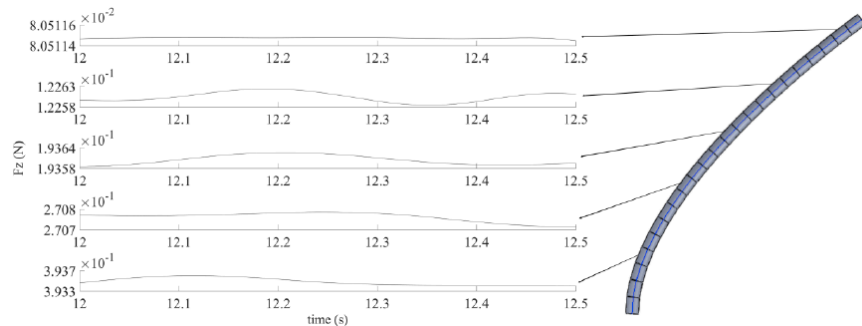


Figure 27: Z-direction drag force on different wall surfaces with times ($v=1.5\text{m/s}$).

frequency and phase migration, it indicates synergetic wake structure effect at two flow regions.

3. CONCLUSION and DISCUSSION

Discussion

This FSI scheme is innovative put forward to simulate the elaborate flow field around cable under a

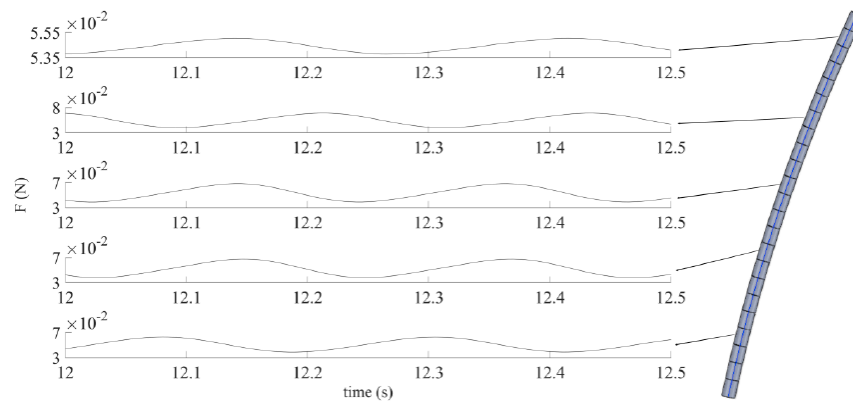


Figure 28: Total drag force on different wall surfaces with times ($v=0.3\text{m/s}$).

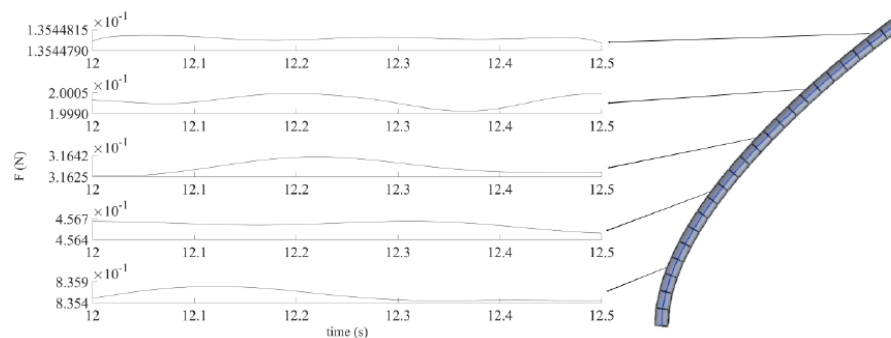


Figure 29: Total drag force on different wall surfaces with times ($v=1.5\text{m/s}$).

laboratory towing condition. It indicates a compact interaction between the cable structure and wake. A transition from elliptical to cylindrical shear layer in a boundary separation is also observed. This transition will draw more grid consistency and accuracy. Vortex induced oscillation can be in a similar spectrum character both in vortex shedding and cable vibrations. However, in a ship trial, A towed cable has a length of 1000m or above. This FSI scheme leads unbearable viscous grid generation. The cable profile has a significant continuity of inclination angle. The dominated elliptical pattern can be made by truncation method to reconstruct an economical and efficient FSI application in a deep diving tow. The stretched length in a short length cable tow or a light weight tow has nonsignificant elongation. However, the shrink of cross section due to cable deform can be a perturbation not a noteworthy hydrodynamic influence.

Conclusion

This paper introduces a flow structure coupling method for towed cable system. Initial cable shape is obtained by NPFEM. Hydrodynamic loads are transferred onto NPFEM cable elements by an innovative transfer method to update the towed cable shape, and final cable shape is obtained by successive substitutions and iterations. The conclusions are drawn as follows:

1. NPFEM coupled with RANS is innovatively established, and this FSI method is validated. This FSI scheme reveals a real strongly hydrodynamic determined cable dynamics and vortex structure induced vibrations around a towed cable system.
2. A method of structured mesh generation of flow field around cable is proposed, and a quasi-static one-way model is applied to a straight tow.
3. Method of selecting fixed drag coefficients for numerical simulation is improved, and the time-averaged FSI method is used to simulate the real underwater motion of towed cable.

This paper suggests a time-averaged FSI method, but there are still a lot of problems that require more investigation. For example, the mesh generation is unstable, when the bending angle of towed cable changes, some areas of mesh need to be adjusted. Another questions like how to use artificial intelligence to help with the construction of the topology of flow field around towed cable, Jeong Hyogu [22] and Freitag Steffen [23] have used neural networks for topology optimization. Further research will consider the transition from time-averaged FSI to transient methods.

REFERENCES

- [1] Kundu P K, Cohen I M, David R. Fluid Mechanics (Fifth Edition) [M] 2012.
- [2] Du X, Cui H, Zhang Z. A numerical method for analyzing the influence of underwater vehicle flow field on dynamic behavior of towed sonar cable array [J]. *Ocean Engineering*, 2019; 175(MAR.1): 163-175. <https://doi.org/10.1016/j.oceaneng.2019.01.047>
- [3] Yang X, Wu J, Xu S. Dynamic analysis of underwater towed system under undulating motion mode of towed vehicle [J]. *Applied Ocean Research*, 2022, 121: 103083. <https://doi.org/10.1016/j.apor.2022.103083>
- [4] Zhao Y, Li G, Lian L. Numerical model of towed cable body system validation from sea trial experimental data [J]. *Ocean Engineering*, 2021, 226(6): 108859. <https://doi.org/10.1016/j.oceaneng.2021.108859>
- [5] Guan G, Zhang X, Wang Y, et al. Analytical and numerical study on underwater towing cable dynamics under different flow velocities based on experimental corrections [J]. *Applied Ocean Research*, 2021; 114: 102768-. <https://doi.org/10.1016/j.apor.2021.102768>
- [6] Wu J, Yang X, Xu S, et al. Numerical investigation on underwater towed system dynamics using a novel hydrodynamic model [J]. *Ocean engineering*, 2022; (Mar.1): 247. <https://doi.org/10.1016/j.oceaneng.2022.110632>
- [7] Grosenbaugh M A. Dynamic Behavior of Towed Cable Systems During Ship Turning Maneuvers [J]. *Ocean Engineering*, 2007; 34(11-12): 1532-1542. <https://doi.org/10.1016/j.oceaneng.2007.01.002>
- [8] Wang Z, Gang S. Parameters influence on maneuvered towed cable system dynamics [J]. *Applied Ocean Research*, 2015; 49: 27-41. <https://doi.org/10.1016/j.apor.2014.10.009>
- [9] Kishore S S, Ganapathy C. Analytical investigations on loop-manoeuvre of underwater towed cable-array system [J]. *Ocean Engineering*, 1998; 25(6): 353-360. [https://doi.org/10.1016/S0141-1187\(97\)00001-1](https://doi.org/10.1016/S0141-1187(97)00001-1)
- [10] Gao, H., Wang, Z. Dynamic Behavior of Two Part Towing Cable System During Turning. *J. Shanghai Jiaotong Univ. (Sci.)* 2018; 23: 444-455. <https://doi.org/10.1007/s12204-018-1928-7>
- [11] Sun F J, Zhu Z H, Larosa M. Dynamic modeling of cable towed body using nodal position finite element method [J]. *Ocean Engineering*, 2011; 38(4): 529-540. <https://doi.org/10.1016/j.oceaneng.2010.11.016>
- [12] Zhu Z H. Dynamic modeling of cable system using a new nodal position finite element method [J]. *Communications in numerical methods in engineering*, 2010; 26(6): 692-704. <https://doi.org/10.1002/cnm.1161>
- [13] IMSL. Users Manual, Math/Library, Fortran Numerical library user's guide math library 7.0. 2016.
- [14] Wilcox D C. Turbulence Modeling for CFD. DCW Industries, 2006.
- [15] C. Geuzaine and JF. Remacle. Gmsh: a three-dimensional finite element mesh generator with built-in pre- and post-processing facilities. *International Journal for Numerical Methods in Engineering* 2009; 79(11): 1309-1331. <https://doi.org/10.1002/nme.2579>
- [16] Huang S. Dynamic analysis of three-dimensional marine cables [J]. *Ocean Engineering*, 1994; 21(6): 587-605. [https://doi.org/10.1016/0029-8018\(94\)90008-6](https://doi.org/10.1016/0029-8018(94)90008-6)
- [17] Wang F, Huang G, Deng D. Dynamic response analysis of towed cable during deployment/retrieval [J]. *Journal of Shanghai Jiaotong University (Science)*, 2008; 13: 245-251. <https://doi.org/10.1007/s12204-008-0245-y>
- [18] Srivastava V K, Sanyasiraju Y, Tamsir M. Dynamic behavior of underwater towed cable in linear profile [J]. *International Journal of Scientific & Engineering Research*, 2011; 2(7): 1-10.
- [19] Park, H. & Jung, Dong & Koterayama, W. (2003). A Numerical and Experimental Study on Dynamics of A Towed Low-Tension Cable. *Applied Ocean Research - APPL OCEAN RES.* 25. 289-299. <https://doi.org/10.1016/j.apor.2004.02.003>
- [20] Wu, Jiaming & Chwang, Allen. (2000). A hydrodynamic model of a two-part underwater towed system. *Ocean Engineering*. 27. 455-472. [https://doi.org/10.1016/S0029-8018\(99\)00006-2](https://doi.org/10.1016/S0029-8018(99)00006-2)
- [21] Rodríguez Luis Á, Armesto J A, Guanche R, et al. Simulation of marine towing cable dynamics using a finite elements method [J]. *Journal of Marine Science and Engineering*, 2020; 8(2): 140. <https://doi.org/10.3390/jmse8020140>
- [22] Jeong Hyogu, Bai Jinshuai, Batuwatta-Gamage C.P., Rathnayaka Charith, Zhou Ying, Gu Yuan Tong. A Physics-Informed Neural Network-based Topology Optimization (PINNTO) framework for structural optimization [J]. *Engineering Structures*, 2023; 278. <https://doi.org/10.1016/j.engstruct.2022.115484>
- [23] Freitag Steffen, Peters Simon, Edler Philipp, Meschke Günther. Reliability-based optimization of structural topologies using artificial neural networks [J]. *Probabilistic Engineering Mechanics*, 2022; 70. <https://doi.org/10.1016/j.probenmech.2022.103356>
- [24] Palacios F, Colonno M R, Aranake A C, et al. Stanford University Unstructured (SU2): An open-source integrated computational environment for multi-physics simulation and design [J]. *AIAA Journal*, 2013; 2013: 1-60. <https://doi.org/10.2514/6.2013-287>

Received on 01-02-2024

Accepted on 13-03-2024

Published on 16-03-2024

DOI: <https://doi.org/10.31875/2409-9848.2024.11.02>

© 2024 Zhi-bo et al.; Zeal Press.

This is an open access article licensed under the terms of the Creative Commons Attribution Non-Commercial License

[\(http://creativecommons.org/licenses/by-nc/4.0/\)](http://creativecommons.org/licenses/by-nc/4.0/), which permits unrestricted, non-commercial use, distribution and reproduction in any medium, provided the work is properly cited.